Nicola J. Ferrier

Mechanical Engineering Department
University of Wisconsin–Madison
1513 University Avenue
Madison, WI 53706 USA
ferrier@engr.wisc.edu

Roger W. Brockett

Division of Engineering and Applied Sciences
Harvard University
29 Oxford Street
Cambridge, MA 02138 USA

Reconstructing the Shape of a Deformable Membrane from Image Data

Abstract

In this paper, we study the problem of determining a mathematical description of the surface defined by the shape of a membrane based on an image of it and present an algorithm for reconstructing the surface when the membrane is deformed by unknown external elements. The given data are the projection on an image plane of markings on the surface of the membrane, the undeformed configuration of the membrane, and a model for the membrane mechanics. The method of reconstruction is based on the principle that the shape assumed by the membrane will minimize the elastic energy stored in the membrane subject to the constraints implied by the measurements. Energy minimization leads to a set of nonlinear partial differential equations. An approximate solution is found using linearization. The initial motivation, and our first application of these ideas, comes from tactile sensing. Experimental results affirm that this approach can be very effective in this context.

KEY WORDS—membrane mechanics, soft fingers, imaging shape

1. Introduction

In this paper, we investigate the theory and application of a new sensing modality based on imaging a deformable membrane. This technique has many potential applications; here we emphasize its applicability to tactile sensing. Deformable membranes are especially suitable for tactile sensing because of their ability to conform to the shape of the object being manipulated, providing compliance and helping to stabilize the grasp. Fluid supported membranes possess desirable force-displacement properties analogous to human finger-

tips (Brockett 1985). Although a number of researchers have experimented with deformable fingers (Akella and Cutkosky 1989; Son, Monteverde, and Howe 1994) and controlled grasp using both the sensed location of contact and the applied force (Chang and Cutkosky 1995; Kao and Cutkosky 1993; Maekawa, Komoriya, and Tanie 1992), the explicit recovery of *shape* does not seem to have been explored (with one exception discussed below). However, if shape information is available, it can be used in the control grasping operations (Montana 1988, 1989). In this paper, we concentrate our efforts on the development of a method to recover the shape of the finger in contact with an object: it is the subject of further work to use this shape information for grasping applications (Hristu 1999).

Using an array of Hall effect sensors and a membrane finger lined with magnets (Nowlin 1991) showed that it is possible to recover shape using the relationship between the change in shape and the change in magnetic field induced by the motion of the magnets. Here we explore the use of imaging to infer the membrane shape. Imaging is advantageous because the sensor can be positioned at some distance from the area of contact and hence can be protected from damage. In addition to its noninvasive nature, imaging is inexpensive and fast enough for a range of applications. This paper shows that the potential drawbacks of imaging, such as computational effort and calibration issues, can be overcome.

Recovering three-dimensional shape from a two-dimensional image requires careful modeling. The popular "shape-from-X" paradigm in computer vision refers to situations in which special assumptions are made about the image formation process and/or the pattern of illumination (examples include shading, structured lighting, controlled motion, and texture). Depth (or equivalently shape) information can be recovered using two or more images of the same scene (Beardsley and

Zisserman 1995; Koenderink and Van Doorn 1991; Tomasi and Kanade 1992; Verri and Torre 1986), two or more images of a moving rigid object (Bennett et al. 1989; Harris 1992), occlusions (Belhumeur 1993), or prior information about the three-dimensional shape of the object (Lowe 1992; Perkins 1978; Terzopoulos, Witkin, and Kass 1987; Ullman and Basri 1991). The tactile sensing application considered here is such that techniques requiring a moving camera are too complex. The membrane is not rigid, and occlusions are usually not present; hence, we must incorporate prior information about the object being imaged, i.e., the membrane.

Here we use what may be termed "shape from elasticity" in conjunction with a classical imaging model. Shape from elasticity minimizes the need for heuristic assumptions about the world. We draw a distinction between this work and the large body of vision/graphics work that makes use of discrete element elastic models for animation and interpretation (see, e.g., Terzopoulos, Witkin, and Kass 1988; Yuille 1990; Lipson et al. 1990), which use deformable models of object to accommodate shape variations and to compensate for projective effects as the viewpoint varies. In our work, we model the physical properties of the elastic material that is being imaged and use this model in the recovery of the 3D shape of an imaged membrane. The shape reconstruction applies to the entire membrane, providing object shape information on that part of the external object that is in contact with the membrane. The idea of imaging a membrane to determine shape has many potential applications beyond this discussion, including its use in laproscopy and tele-medicine.

In the following section, we briefly describe the imaging model. Then we describe a mathematical model that is based on the elastic energy associated with a membrane under deformations from a known nominal position. The minimum energy solution combined with boundary, volume, and image constraints leads to a set of nonlinear partial differential equations. Using grid approximations, we solve a linearized form of these equations. Finally, we give some experimental results of the membrane shape reconstruction algorithm.

2. Description of the Physical Setup

A prototype of the class of problems under discussion here is shown in Figure 1. The imaging configuration is well-defined: we image the surface of a membrane that forms part of the boundary of a fluid-filled cavity. A pattern of dots has been drawn on the interior surface of the membrane. The pattern to be imaged and the light source are part of the sensor design. Because the fluid in the cavity is essentially incompressible, the volume contained within the cavity is constant.

The physics of the situation can be characterized as follows

(1) Displacements of portions of the membrane arising from contact with external contacts that distort the shape of the membrane. The portion of the membrane that is *not* in contact with the external objects deforms in such a way to minimize the elastic energy stored in the "free" portion of the membrane.

(2) The volume contained within the membrane cavity is constant.

(3) The boundary of the membrane is fixed, and the remaining components defining the cavity have a fixed geometry.

(4) A large number of points on the inside of the membrane are imaged. A suitable approximation of the nominal (undeformed) position of the membrane is known from prior calibration.

(5) The displacements of the dots on the image plane are observed.

We use a pinhole projection model for the image formation process. A coordinate frame is chosen (see Fig. 2) such that a point with coordinates (x, y, z) projects to image point (u, v):

$$u = -f\frac{x}{z}, \quad v = -f\frac{y}{z}, \tag{1}$$

where f is the distance from the image plane to the pinhole.

Suppose that under deformation the membrane pattern distorts and the coordinates of a pattern point change from (x, y, z) to (x', y', z'). The imaging equation yields the following:

$$(x', y', z') = \left(z'\left(\frac{u + \delta u}{-f}\right), \quad z'\left(\frac{v + \delta v}{-f}\right), \quad z'\right), \tag{2}$$

where (u, v) are the image position of the dots on the membrane before the distortion and $(\delta u, \delta v)$ are the measured image displacements of the dots on the membrane after the distortion.

It is crucial to know the a priori position of the dots on the membrane with reasonable accuracy. In the application presented here, the membrane dot pattern is drawn on the membrane using a CNC milling machine and the relationship between the dots and the camera is established using a calibration procedure, to be described later. Under distortion, the positions of each dot on the membrane are determined from its projection in the image, up to a scaling factor (i.e., the depth, z'). The central issue here is the recovery of the scaling factor.

3. Membrane Shape Reconstruction

Elementary treatments of the continuum mechanics of membranes discuss small deformations of a flat membrane subject to fixed boundary support. The situation of interest here is more complicated because the unstretched membrane is not flat, the region of deformation is not simply connected, and
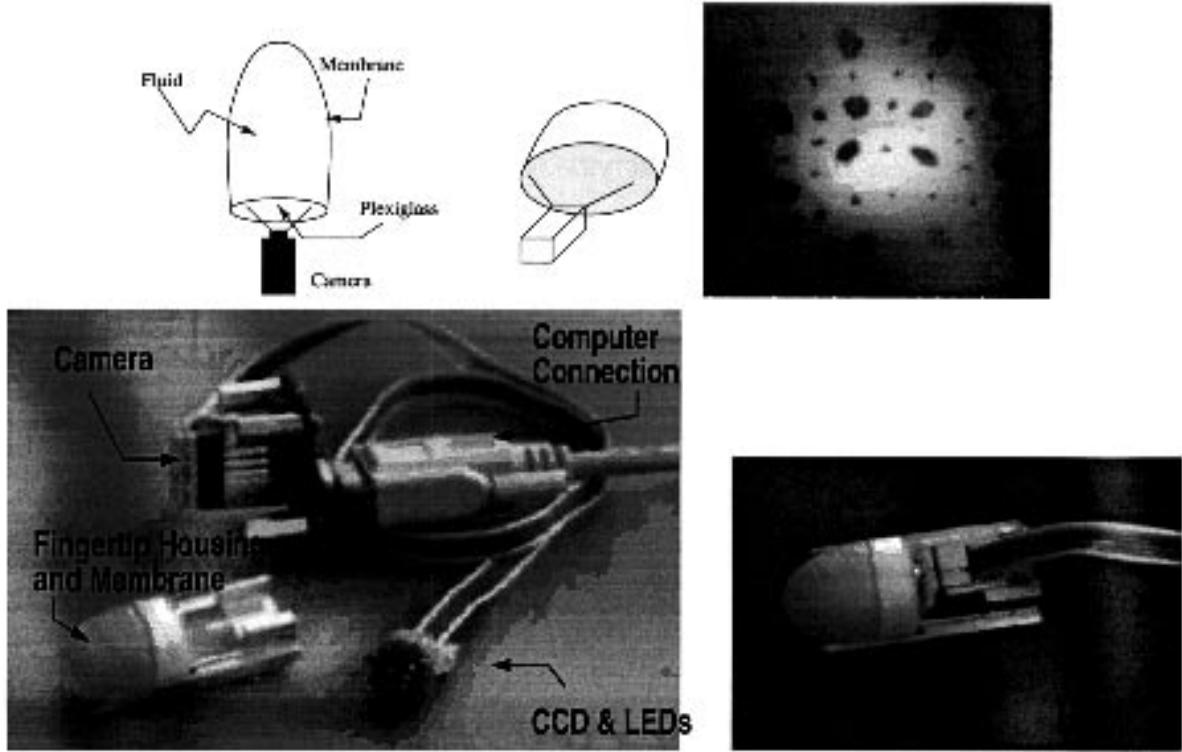
Fig. 1. (a)A graphical depiction of imaging configuration, (b) a typical image of the inside of the membrane, (c) the device in pieces with the individual components indicated, and (d) a photograph of the actual device.
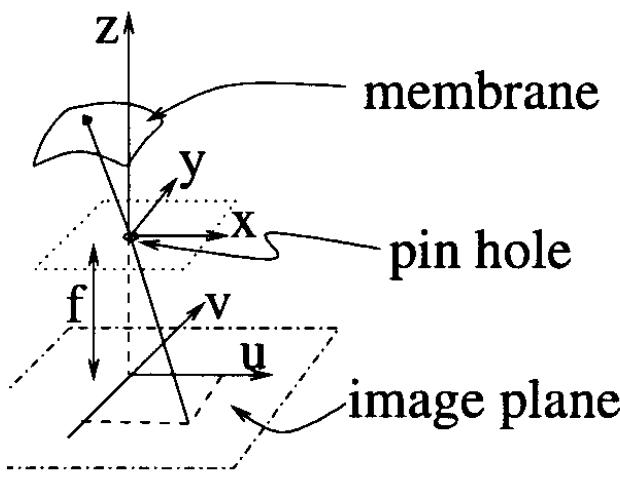

Fig. 2. Coordinate convention for imaging/membrane.

the mechanics impose a constraint on the "volume" of the deformation. We ignore the thickness of the membrane and any consideration of bending stiffness. Let the surface of the undeformed membrane be identified with a manifold M. Think of M as a Riemannian manifold with metric inherited from ordinary three-dimensional space. The postdeformation surface is identified with a manifold N; the mapping

$$\phi : M \to N \qquad (3)$$

describes the displacement of the material points that make up the membrane. For a given N, it is known that the map ϕ that minimizes the elastic energy is a harmonic map from M to N (defined below) provided that the membrane does not wrinkle. Such maps are characterized as the solution of a set of nonlinear partial differential equations, or, equivalently, as the minimizers of the harmonic map functional

$$E(\phi) = \frac{1}{2} \int_M \mathrm{tr}[J^T(\phi) H J(\phi) G^{-1}] dV_M - E_0, \qquad (4)$$

where $J(\phi)$ is the Jacobian of ϕ, dV_M is the volume element on M, G is the Riemmanian metric on M, H is the Riemmanian metric on N, and E_0 is the energy associated with the undeformed membrane. For deformations that stretch the membrane, this expression is a suitable model of the elastic

stored energy (Eells and Lemaire 1978; Eells and Sampson 1964). More discussion is given in Appendix B. The expression for $E(\phi)$ shows that if N is known, then the elastic energy can be computed from a knowledge of the material point deformations through a suitable linearization expressed here as J. Although not immediately apparent, one may think of this expression for energy as being the sum of the squares of local changes in lengths along the two principal axes of the deformations. It must be emphasized, however, that in the applications we are discussing that the characterization of ϕ will only be a means to an end because N will not be known in advance. In fact, the determination of ϕ is of less interest than the determination of N, but in our situation these must be determined jointly.

3.1. The Elastic Energy

To proceed, we parameterize the space of deformations and use a discrete approximation for $E(\phi)$. This will let us find an approximation to N while finding ϕ. We will then use the constraints imposed by the imaging and the constraints on the volume of the cavity defined by the membrane and the housing as data for an algorithm. As in Section 2, we use a coordinate system with the origin along the optical axis. The xy plane of this coordinate system coincides with a certain part of the boundary of the cavity, and the membrane can be identified with a surface above this plane (see Fig. 3(a)). We need to consider separately the specification of the shape of the membrane and the specification of the displacements of material points.

To describe the shape, we specify the z-coordinate, z_{ij} associated with the point on the undeformed membrane lying above (x_{ij}, y_{ij}) on the xy plane. This is not a material point. We take as our description of M, thought of as a submanifold of $\mathbb{R}^3$, as

$$M = \{x, y, z \mid x = x; \ y = y; \ z = s(x, y)\} \qquad (5)$$

and describe its deformed version, N, as

$$N = \{x, y, z \mid x = x; \ y = y; \ z = s(x, y) + \psi(x, y)\}, \quad (6)$$

that is, the shape function for the undeformed membrane is $s(x, y)$ and the surface map of the deformed membrane is $s(x, y) + \psi(x, y)$, where $\psi(x, y)$ is the incremental shape function. Our goal is to find the incremental shape map ψ, but, as noted above, we will need to find the material point map ϕ in this process (Fig. 3 b,c) because we observe the motion of material points on the membrane.

Under distortion, a point on the membrane with coordinates (x, y, z) will displace, moving according to the material point map

$$\hat{\phi}(x, y, s(x, y)) = (x', y', s(x', y') + \psi(x', y')). \qquad (7)$$

ϕ is a mapping of manifolds, and we use $\hat{\phi}$ to denote the mapping in our specified coordinates. An $m \times n$ grid is defined

on the xy plane. In the undeformed state, the projection along the z-axis of the grid onto the membrane divides the membrane into curvilinear quadrilaterals (Fig. 3(a)). The grid is distinct from, and of finer resolution than, the dot pattern placed on the membrane for the purpose of imaging (see Fig. 4(b)). For the sake of brevity, we drop the adjective curvilinear and refer simply to *quadrilaterals* throughout the remainder of this paper. We index the quadrilaterals by the grid indices $i, j, i = 1, \dots, n, j = 1, \dots, m$. Define the set

$$\mathcal{B}_{ij} = \{(i, j), (i + 1, j), (i + 1, j + 1), (i, j + 1)\}. \quad (8)$$

By the ijth quadrilateral, we mean the quadrilateral with vertices at grid indices in the set $\mathcal{B}_{ij}$. We consider the approximation of $\hat{\phi}$ by a family of locally affine maps sending the undeformed quadrilaterals to the deformed ones. We approximate ϕ in the ijth quadrilateral by an affine map with linear part, A_{ij}, and translation part, b_{ij}. Table 1 summarizes the language and notation we are using.

An expression for the energy associated with a material point displacement map, ϕ, and a manifold N has already been given; it contains G and H, the metrics on M and N. These metrics can be expressed in terms of the partial derivatives of of the shape functions s and ψ,

$$G = \begin{bmatrix} 1 + (s_x)^2 & s_x s_y \\ s_x s_y & 1 + (s_y)^2 \end{bmatrix} \qquad (9)$$

$$H = \begin{bmatrix} 1 + (s_x + \psi_x)^2 & (s_x + \psi_x)(s_y + \psi_y) \\ (s_x + \psi_x)(s_y + \psi_y) & 1 + (s_y + \psi_y)^2 \end{bmatrix}. \qquad (10)$$

This makes evident the fact that contributions to the elastic energy are coming from a repositioning of material points, ϕ, and contributions from a change in the shape, $(s_x, s_y, \psi_x, \psi_y)$. Recall that the expression for the energy is

$$E = \int \int \text{tr} \left[\frac{\partial \phi}{\partial \mathbf{x}}^T H \frac{\partial \phi}{\partial \mathbf{x}} G^{-1} \right] dx dy, \quad \mathbf{x} = (x, y)^T. \quad (11)$$

LEMMA 1. The change in energy associated with a material point map ϕ and an incremental shape change map ψ is given, in the neighborhood of an equilibrium configuration, by

$$E(\phi, \psi) \approx \sum_{ij} \left[\text{tr} A_{ij}^T H A_{ij} G^{-1} \ area_{ij} \right] + \xi, \qquad (12)$$

Table 1. Summary of the mappings

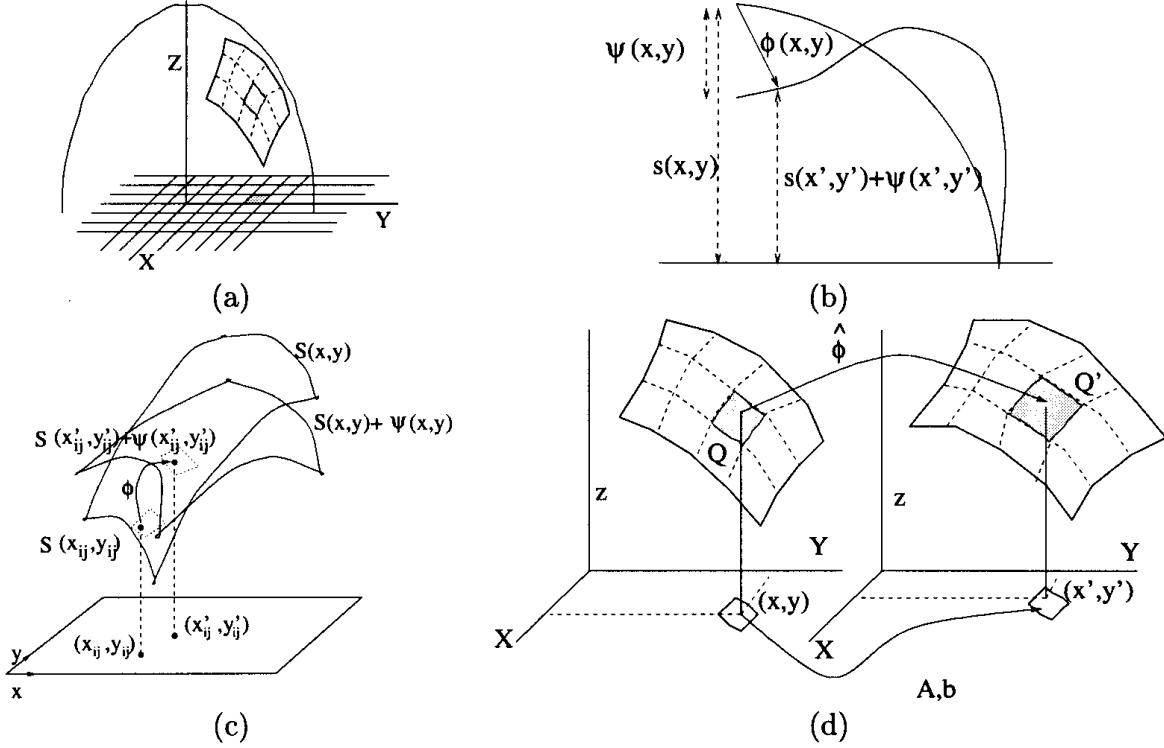|	
$\phi : M \to N$	material displacement map
$s : \mathbb{R}^2 \to \mathbb{R}$	shape function
$\psi : \mathbb{R}^2 \to \mathbb{R}$	incremental shape function
$\hat{\phi} : \mathbb{R}^3 \to \mathbb{R}^3$	coordinate representation of ϕ
$A_{ij} : \mathbb{R}^2 \to \mathbb{R}^2$	approximation to ϕ (local affine maps)

Fig. 3. (a) Extrinsic representation of the membrane as a surface in R^3. A grid on the xy plane divides the membrane into quadrilateral elements. (b) ϕ is used to recover ψ. The new shape, $s(x', y') + \psi(x', y')$, is found from the nominal shape, $s(x, y)$, and the material displacement, $\phi(x, y)$. The diagram shows these mappings in the plane (b) and in 3-space. (c) Note that A, the approximation to ϕ, is the projection of material displacement, ϕ. (d) A local linear approximation to ϕ maps quadrilaterals to quadrilaterals. For clarity, only a portion of the membrane is shown.

where the area terms are

$$area_{ij} = \sqrt{(1 + s_x^2)(1 + s_y^2) - s_x^2 s_y^2} \tag{13}$$
$$\cdot (x_{i+1\ j} - x_{i\ j})(y_{i+1\ j} - y_{i\ j}),$$

A_{ij} is as above, and ξ is of third order.

We will now use this lemma to derive an expression showing how the energy depends on the data that define the parameters of the affine approximation, A_{ij} and b_{ij}. Let ψ_{ij} be the value of ψ at the grid points (x_{ij}, y_{ij}) and use discrete approximations to the partial derivatives in eq. (10). The partial derivatives $[\psi_x, \psi_y]$ at the grid indexed by ij are expressed in terms of ψ_{ij}, $\psi_{i+1\ j}$, $\psi_{i+1\ j+1}$, and $\psi_{i+1\ j+1}$. Define the vector $\hat{\psi} = [\psi_{11}, \ldots, \psi_{1n}, \ldots, \ldots, \psi_{mn}]$ whose components are discrete values of the incremental shape map, indexed by their grid position. Once $\hat{\psi}$ is determined, we have a discrete approximation of the shape of N.

With finite difference approximations to the partial derivative terms and with the elements of A_{ij} in eq. (12), the approximate formula for E can be organized in terms of the sum of quadratic terms in the incremental shape function, ψ_{ij}, and quadratic terms in the approximation to the material point

mapping, plus higher order terms, which we will ignore. By incorporating the contributions from each quadrilateral, we can rewrite our approximation for the energy as a quadratic form in the incremental shape change as represented by $\hat{\psi}_{ij}$ (see Appendix D for details)

$$E(\hat{\psi}) = \|\tilde{Q}\hat{\psi} - \boldsymbol{\gamma}\|^2, \tag{14}$$

where the terms of $\tilde{Q}$ depend on the shape of the nominal membrane as reported by $s(x, y)$ and the approximation to the material displacement map, ϕ.

3.2. Elastic Energy with the Image Constraints

Interpolation of the imaged motion of the observed material points gives us an approximation to $\hat{\phi}$. The motion of this pattern is the projection of ϕ. For interpolation of the image flow, we use least squares matching. Given the image coordinates $p_{kl} = (x_{kl}, y_{kl})$ and $p'_{kl} = (x'_{kl}, y'_{kl})$, a local linear approximation to ϕ is described by A_{ij}, b_{ij} where A, b will be chosen according to

$$A_{ij}, b_{ij} = \overset{\text{argmin}}{\underset{A,b}{}} \sum_{kl \in \mathcal{B}_{ij}} \|(Ap_{kl} + b) - p'_{kl}\|^2, \tag{15}$$
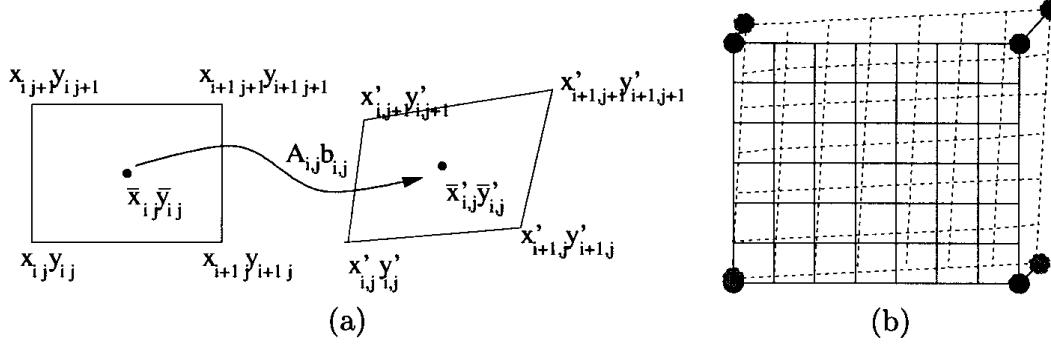
Fig. 4. (a) An affine approximation is used to describe motion of the projection of each quadrilateral on the plane. (b) The motion of the material points (large dots) is observed. A finer resolution grid is used for discrete approximations.

where $\mathcal{B}_{ij}$ was defined in eq. (8). Let

$$F_{ij} = \left(\sum_{kl \in \mathcal{B}_{ij}} p_{kl} \cdot (p'_{kl})^T \right) - 4 \bar{p}_{ij} (\bar{p}'_{ij})^T \quad \text{and}$$

$$G_{ij} = \left(\sum_{kl \in \mathcal{B}_{ij}} p_{kl} \cdot p_{kl}^T \right) - 4 \bar{p}_{ij} \bar{p}_{ij}^T, \tag{16}$$

where $\bar{p}_{ij}$ denotes the centroid of the ijth quadrilateral. The best fit is given by (see Appendix C)

$$A_{ij} = F_{ij}^T G_{ij}^{-1} \quad \text{and} \quad b_{ij} = A_{ij} \bar{p}_{ij} - \bar{p}'_{ij}. \tag{17}$$

Note that G_{ij} depends on the coordinates of the dot pattern on the membrane in the *undeformed configuration*, and thus G_{ij}^{-1} can be computed off-line. F_{ij} depends on the coordinates of the dot pattern on the membrane in the *deformed configuration*, which reveals its dependence on the incremental shape map, ψ.

The energy associated with a given image displacement and a given incremental shape map, $\hat{\psi}$, becomes, in this way, a function of the measured image displacement. Using the above expressions, $\tilde{Q}$, which depends on A_{ij}, is re-expressed in terms of the image flow measurements $(\delta u_{ij}, \delta v_{ij})$,

$$E(\delta u, \delta v) = \| Q(\delta u, \delta v) \hat{\psi} - \boldsymbol{\gamma} \|^2. \tag{18}$$

The imaging constraints are incorporated into the definition of the $nm \times 1$ vector $\boldsymbol{\gamma}$ and the matrix Q. The entries in Q and $\boldsymbol{\gamma}$ are functions of the nominal membrane position $(x, y, s(x, y))$, the image displacements $(\delta u, \delta v)$, and the imaging parameters. If the image displacement is zero, then $\boldsymbol{\gamma}$ is zero and hence the minimum energy solution will be $\hat{\psi} = 0$.

3.3. Volume Constraint

A displacement of the membrane does not change the volume enclosed by the membrane, and we assume that the

boundary of the membrane lies entirely within the xy plane. The volume enclosed by the membrane can be computed by splitting each quadrilateral into two triangles and identifying with each triangle a tetrahedron with one vertex being the origin. For quadrilateral, q_{ij}, one such tetrahedron is described by the vertices $[x_{ij}, y_{ij}, z_{ij}]$, $[x_{i\ j+1}, y_{i\ j+1}, z_{i\ j+1}]$, $[x_{i+1\ j+1}, y_{i+1\ j+1}, z_{i+1\ j+1}]$, and $[0, 0, 0]$. The volume of this tetrahedron is given by

$$V = \frac{1}{6} \begin{vmatrix} x_{ij} & y_{ij} & z_{ij} \\ x_{i\ j+1} & y_{i\ j+1} & z_{i\ j+1} \\ x_{i+1\ j+1} & y_{i+1\ j+1} & z_{i+1\ j+1} \end{vmatrix} \triangleq \frac{1}{6} \det C_{ij}, \tag{19}$$

where C_{ij} is defined to be the matrix whose rows are the coordinates of the vertex points ordered as indicated. The volume contained within the membrane is approximated by the sum of the volumes of the tetrahedra. If a vertex of the tetrahedron element is given in terms of a right-handed Cartesian coordinate system, then equations are valid only when nodes are numbered in a counterclockwise manner when viewed from the origin (see Fig. 5).

We now determine the effect of a small displacement of the vertices has on the volume. The volume, V' of the tetrahedral element after distortion that sends C into $C + \delta C$ is given by

$$V' = \frac{1}{6} (\det[C + \delta C]) = \frac{1}{6} \left(\det \left[C(I + C^{-1} \delta C) \right] \right)$$

$$\approx \frac{1}{6} \det C (1 + \text{tr}[C^{-1} \delta C])$$

$$= \frac{1}{6} \det C \left(1 + \frac{1}{\det C} \text{tr}[\text{adj} C\, \delta C] \right)$$

$$= \frac{1}{6} \det C + \frac{1}{6} \text{tr}[\text{adj} C\, \delta C].$$

Hence, the change in volume is approximated by

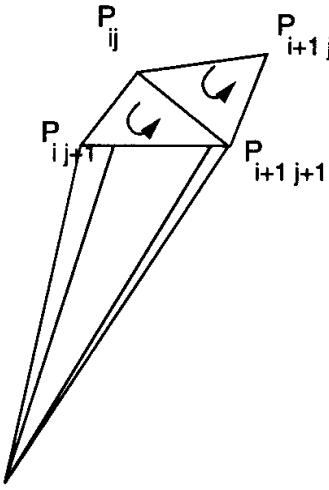$$\Delta V \approx \frac{1}{6} \text{tr}[\text{adj} C\, \delta C], \tag{20}$$

Fig. 5. The computation of the volume of the membrane is reduced to a computation of the volume of tetrahedral elements. The arrows depict the order that the vertices must be taken to compute volume.

where adj$C$ is the classical adjoint of C (i.e., the matrix of signed cofactors) and δC is the matrix with elements that are the change in coordinates of the membrane. Notice that the matrix adj$C$ is a function of nominal membrane position and can be computed off-line. The trace operation is linear and hence the expression $\Delta V = 0$ is linear in the elements of δC.

The total change in volume is given by the sum of the changes in volume for each tetrahedron and is also a linear expression in the elements of δC. We use the imaging constraints (eq. (2)) to express the elements of δC in terms of the nominal positions $(x_{ij}, y_{ij}, s(x_{ij}, y_{ij}))$, the measured image displacements $(\delta u_{ij}, \delta v_{ij})$, and the unknowns $\hat{\psi}_{ij}$. This can be expressed in terms of the vector $\hat{\psi}$, leading to an equation of the form

$$\mathbf{v}^T \hat{\psi} - c = 0. \tag{21}$$

4. The Algorithm

The discrete approximations presented in the previous sections allow us to formulate the membrane shape reconstruction problem as finding the value of $\hat{\psi}$ that satisfies the following expression

$$\hat{\psi}_{min} = \min_{\hat{\psi}} \tfrac{1}{2} \|Q\hat{\psi} - \boldsymbol{\gamma}\|^2, \quad \text{subject to } \mathbf{v}^T \hat{\psi} - c = 0, \quad \text{and} \quad \hat{\psi}_{ij} = 0 \text{ for grid indices } (i, j) \text{ on the boundary.}$$

This is a constrained minimization problem with solution

$$\hat{\psi} = \left(Q^T Q\right)^{-1} Q^T \boldsymbol{\gamma}$$
$$+ \left(\frac{c - \mathbf{v}^T \left(Q^T Q\right)^{-1} Q^T \boldsymbol{\gamma}}{\mathbf{v}^T \left(Q^T Q\right)^{-1} \mathbf{v}}\right) \left(Q^T Q\right)^{-1} \mathbf{v}. \tag{22}$$

To arrive at this expression, we needed to reduce $\hat{\psi}$ by the removal of the boundary data terms ($\hat{\psi}_{ij} = 0$). The reduced incremental shape map vector is denoted by $\tilde{\psi}$. We solved a modified reconstruction problem

$$\min_{\tilde{\psi}} \ \|Q\tilde{\psi} - \boldsymbol{\gamma}\|^2 \quad \text{subject to } \mathbf{v}^T \tilde{\psi} - c = 0 \tag{23}$$

for the remaining components of $\hat{\psi}$. The minimization problem is solved using Lagrange multipliers:

$$L(\psi, \lambda) = \frac{1}{2}(Q\psi - \boldsymbol{\gamma})^T (Q\psi - \boldsymbol{\gamma}) + \lambda(\mathbf{v}^T \psi - c) \tag{24}$$
$$= \frac{1}{2}\psi^T Q^T Q\psi - \boldsymbol{\gamma}^T Q\psi + \frac{1}{2}\boldsymbol{\gamma}^T \boldsymbol{\gamma} + \lambda(\mathbf{v}^T \psi - c),$$

where λ is a Lagrange multiplier, not to be confused with the elastic constant used earlier. Equating the derivatives L_ψ, L_λ to zero gives

$$0 = Q^T Q\psi - Q^T \boldsymbol{\gamma} + \lambda \mathbf{v} \tag{25}$$
$$0 = \mathbf{v}^T \psi - c. \tag{26}$$

We solve eq. (25) for ψ: $\psi = \left(Q^T Q\right)^{-1} \left(Q^T \boldsymbol{\gamma} - \lambda \mathbf{v}\right)$ and substitute the result into eq. (26), then solve for λ:

$$\lambda = \frac{\mathbf{v}^T \left(Q^T Q\right)^{-1} Q^T \boldsymbol{\gamma} - c}{\mathbf{v}^T \left(Q^T Q\right)^{-1} \mathbf{v}}. \tag{27}$$

Using this value of λ in eq. (25) yields eq. (22).

The minimization problem reduces to solving a least squares problem (eqs. (25) and (26)). This problem formulation involved approximations in expressing the volume linearly and the energy as a quadratic. Obviously, the accuracy of the reconstruction depends on the accuracy of these approximations.

Because the discrete expression for the energy was derived using a local approximation to the deformation on a coarse scale, the solution may not be smooth. To enforce continuity of the resulting solution, as is common in solving stiff differential equations, we modify the quadratic form to be

$$\|(\mathbf{Q} + \mathbf{S})\psi\|^2, \tag{28}$$

where $\psi^T \mathbf{S}^T \mathbf{S}\psi$ is a discrete approximation to the square of the Laplacian.

5. Implementation and Results

We have applied the analysis given above to a membrane tactile sensor. A prototype device is shown in Figure 1, and a second generation device is shown in Figure 14. A pattern of dots is drawn on the interior surface of the membrane. The membrane surface is imaged through a 50 micron pinhole using a CCD camera. In practice, we used patterns on the order of 10×10 dots, alternating small and large dots as shown in Figure 1(b).

The dots are detected using a gray scale thresholding operation and a connected component analysis (standard image operations as described in, e.g., Horn 1986). Under deformation, the dots move and the image displacement is measured using a heuristic search based on both proximity and dot size. There are two sizes of dots to enable "multi-scale" matching, which improves the speed and provides matching accuracy.

As described earlier, our measurements are of the displacements of the projected dot pattern after deformation. To use discrete approximations described above, we require the projected flow at the grid vertices; hence, we used bilinear interpolation to approximate the projected material deformation at the grid vertices. Typical results are shown in Figure 6.

5.1. Segmentation of Contact Location

It is important that we segment the points on the membrane that are in contact with the object from those that are not in contact because only the "free" portion of the membrane will distort in such a way that the elastic energy is minimized (see Section 4 and appendix B). For nonpoint contacts, shape reconstruction requires knowledge of the shape of the object (Elliott and Friedman 1986). Here we restrict to the case of point contacts. At the contact location, the derivatives of the shape function can have discontinuities.

To determine the approximate location of contact, we analyze the the image displacement field. Using the notation of Section 2, we compute the change in polar angle for each imaged material point

$$d\beta = \beta_0 - \beta_1 < 0, \qquad (29)$$

where

$$\beta_0 = cos^{-1}(\frac{f}{\sqrt{u^2 + v^2 + f^2}})$$

$$\beta_1 = cos^{-1}(\frac{f}{\sqrt{(u + \delta u)^2 + (v + \delta v)^2 + f^2}})$$

and f is the a focal distance (see Fig. 7). $d\beta$ is zero at the boundary. If $d\beta$ is positive in a neighborhood of the boundary, then that region "bulges out." The change of $d\beta$ from positive to negative indicates regions of contact when the contact force is along the surface normal. The sign of $d\beta$ determines whether the angle between the surface normal and the optical axis increases or decreases. If the applied force is directly along the optical axis (a nongeneric situation), then the flow is everywhere divergent. This is readily detected, and the optical axis is chosen as the contact location.

If the contact is not directed along a ray normal to the membrane surface, which typically will be the situation, then the image flow may not yield sufficient information to compute the contact location. One must know the surface normal before and after the contact has been applied. However, the surface normal of the deformed membrane can only be computed after the shape has been reconstructed. Thus, we must resort to an iterative reconstruction/segmentation process that reconstructs the membrane with a contact location estimated as above, then computes the corresponding contact location using the reconstructed shape. Some indentors may cause occlusion, a situation we do not analyze here.

Figure 8 presents the results of the initial segmentation algorithm. Figures 9 and 10 show the detection of one and two contact locations using the iterative procedure.

5.2. Calibration of the Nominal Membrane Position

A crucial element of our reconstruction method is the assumption that the nominal positions of the membrane dots (in three dimensions) are given. To obtain this nominal position, we establish the location on the image of a desired dot pattern. Using ray-tracing optics and taking into consideration the indices of refraction of both the Plexiglas and water, we computed the intersection of a ray originating at a specific location with the image plane. The recorded positions of a set of such locations were used to position points on the membrane using a CNC mill. A calibration was used to null small errors in the construction process.

5.3. Reconstruction Results

We implemented our reconstruction algorithm using commercially available imaging equipment. Although we do not give details here, the reconstruction computation takes advantage of properties of Q, and much of the computation required to evaluate the expression in eq. (22) can be performed in advance (using the nominal values of the membrane position and focal length). During run-time, we acquire an image of the membrane under deformation, process the image to locate the dots, measure the image displacement of the dots as described earlier, and use this to perform the reconstruction using eq. (22).

Using a 200 MHz Pentium-Pro computer with Epix framegrabber, Elmo camera, and a fiber-optic light source, the shape reconstruction algorithm time has been reduced to approximately 200 ms hence performing shape reconstruction at about 5 Hz. A second generation "finger" tactile sensor using the improved imaging equipment is shown in Figure 14.

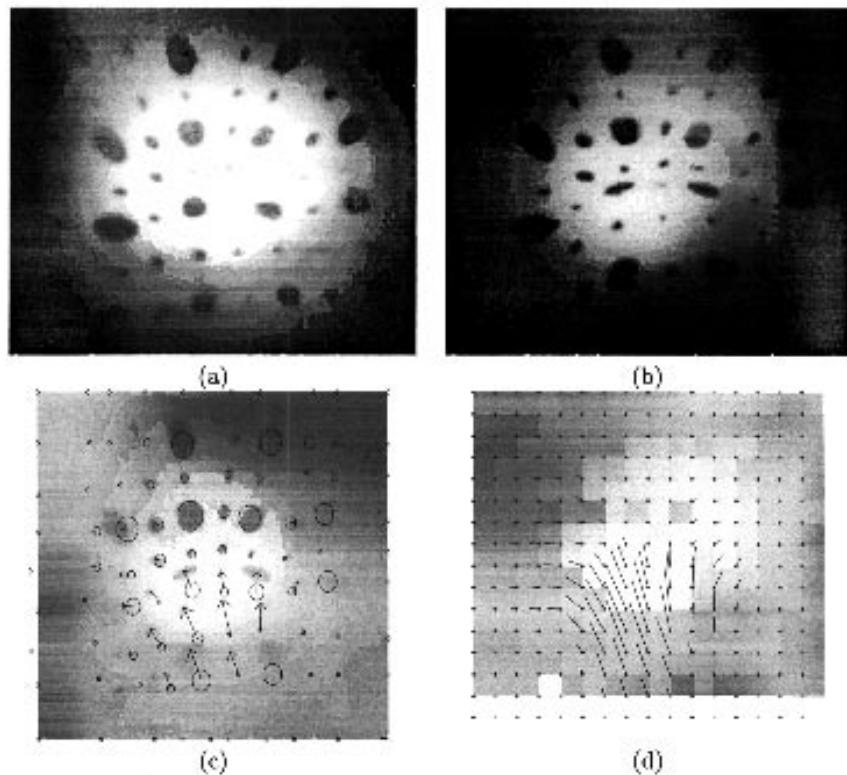Figures 12-13 present examples of results of the reconstruction of the membrane under deformation. Part (a) of

Fig. 6. (a) Image of undeformed membrane, (b) image of the distorted membrane, (c) the measured flow vectors overlaid on the undeformed image, and (d) an equivalent 16×16 interpolated flow field (vectors are magnified).
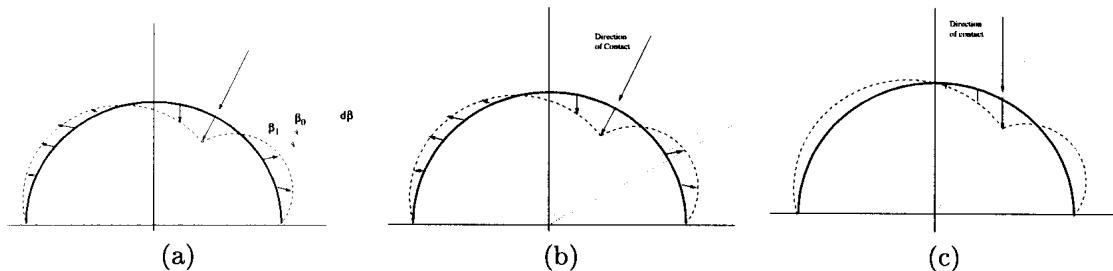

Fig. 7. (a) Cartoon depiction of the segmentation computation variable $d\beta$. (b) Typical deformation when the contact is along a radial line. (c) Contact location is incorrect when the contact is not radially directed.
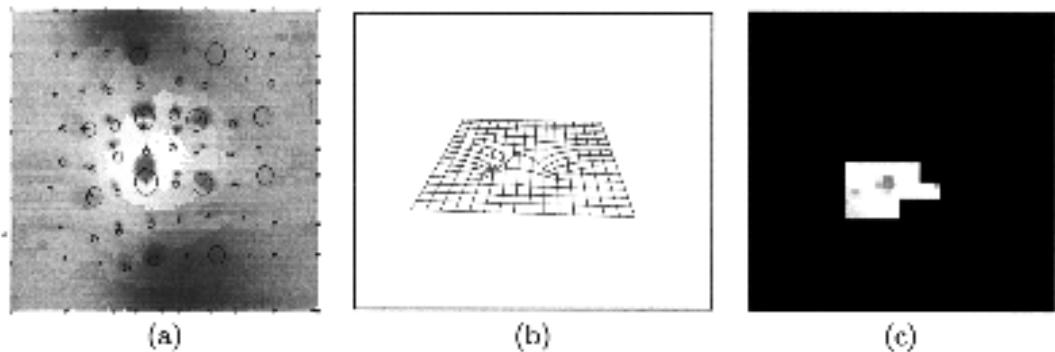
Fig. 8. (a) Image of distorted membrane with graphic representation of image motion of the dots overlaid. (b) Graphic representation of $d\beta$. (c) Segmentation of contact location—location is taken as the centroid of the region that "bulges in."
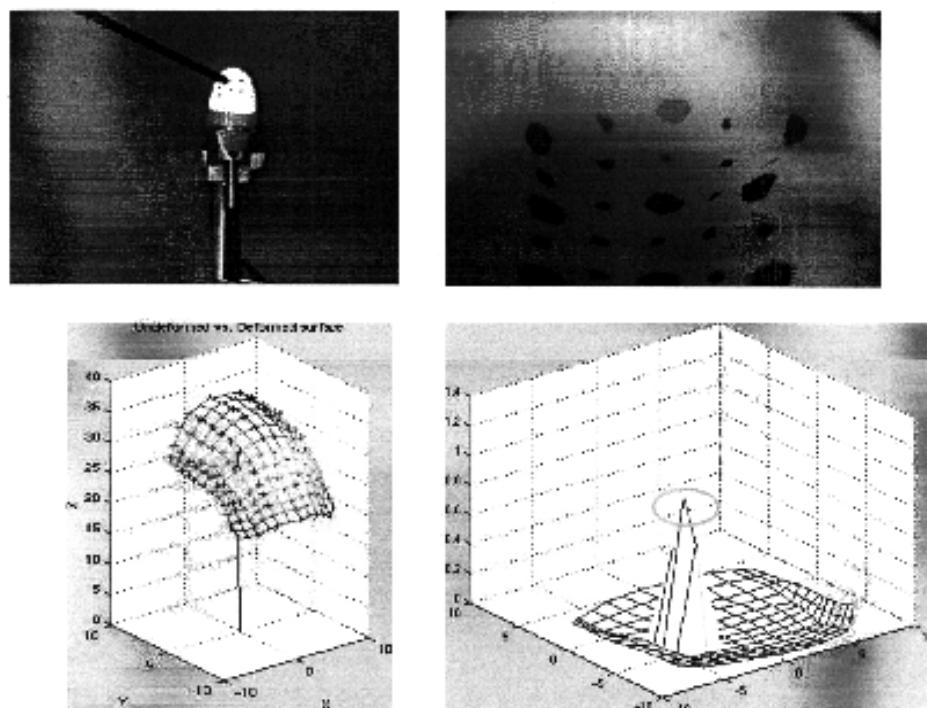
Fig. 9. Example of detection of location of contact for a single indentor. An iterative procedure is used to detect the contact location and perform reconstruction (see text).
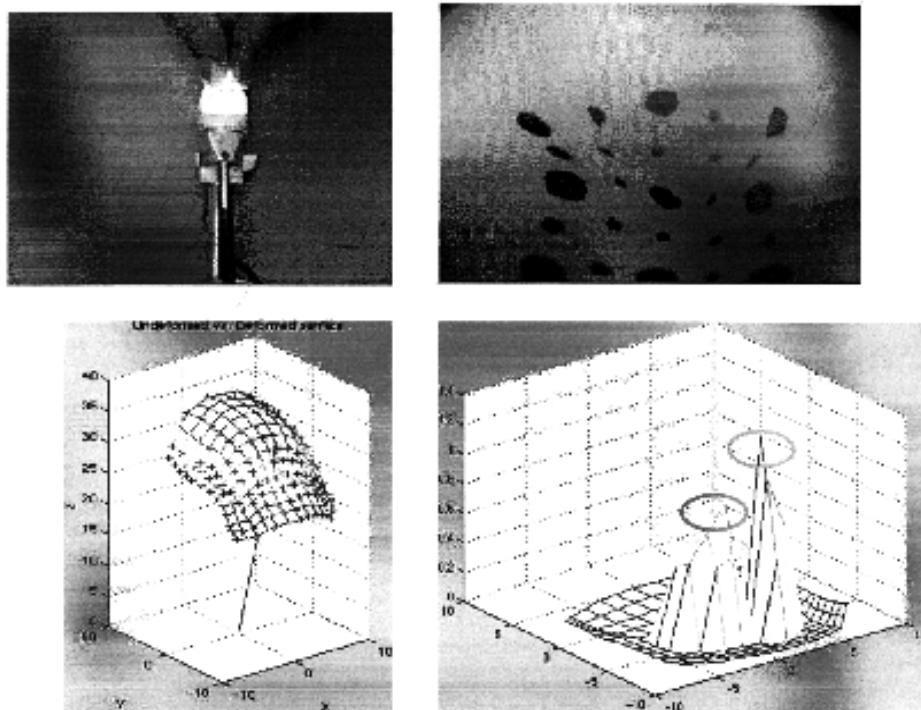
Fig. 10. Example of detection of location of contact for two indentors. An iterative procedure is used to detect the contact location and perform reconstruction (see text).
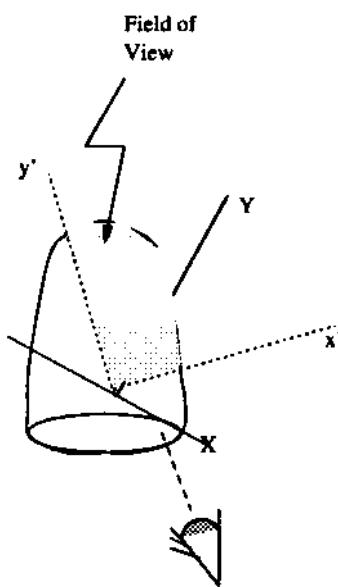

Fig. 11. The viewpoints used for the reconstruction results represented. Figure 12 views the membrane from the side using the $x' - y'$ axes shown. Figure 13 presents the reconstructed finger viewed down the length of the finger as depicted with the "eye" shown here.

each figure shows the image of the membrane under deformation. Part (b) shows the superposition of the undeformed image with the displaced blob positions (as viewed in part (a)) indicated. The circles are drawn where the blob appears in the undeformed membrane image, and the arrows depict the image displacement of the projected blob from the undeformed membrane (the tail of the arrow) to the deformed membrane (the head of the arrow). This image displacement is used as input, along with our physical constraints to solve the system of eqs. (22). The resulting reconstructed finger shape is shown in (c). The cross marks (+) indicate the original membrane position. The mesh is our reconstruction of the membrane shape. In Figure 12, the reconstruction is a side view of the membrane. The membrane was contacted with a point indenter (the end of a pen). In Figure 13, the reconstruction is an end view of the finger (i.e., viewing the finger down its length). In Figure 13, the membrane was squeezed on the side. In the last result, shown in Figure 13, the membrane was squeezed on both sides. We capture both contacts successfully.

Figure 15 shows membrane shape reconstruction using the finger shown in Figure 14. The addition of a fiber-optic light source facilitates imaging over a larger membrane surface area.

Figure 16 demonstrates poor performance when the image flow is incorrectly measured.
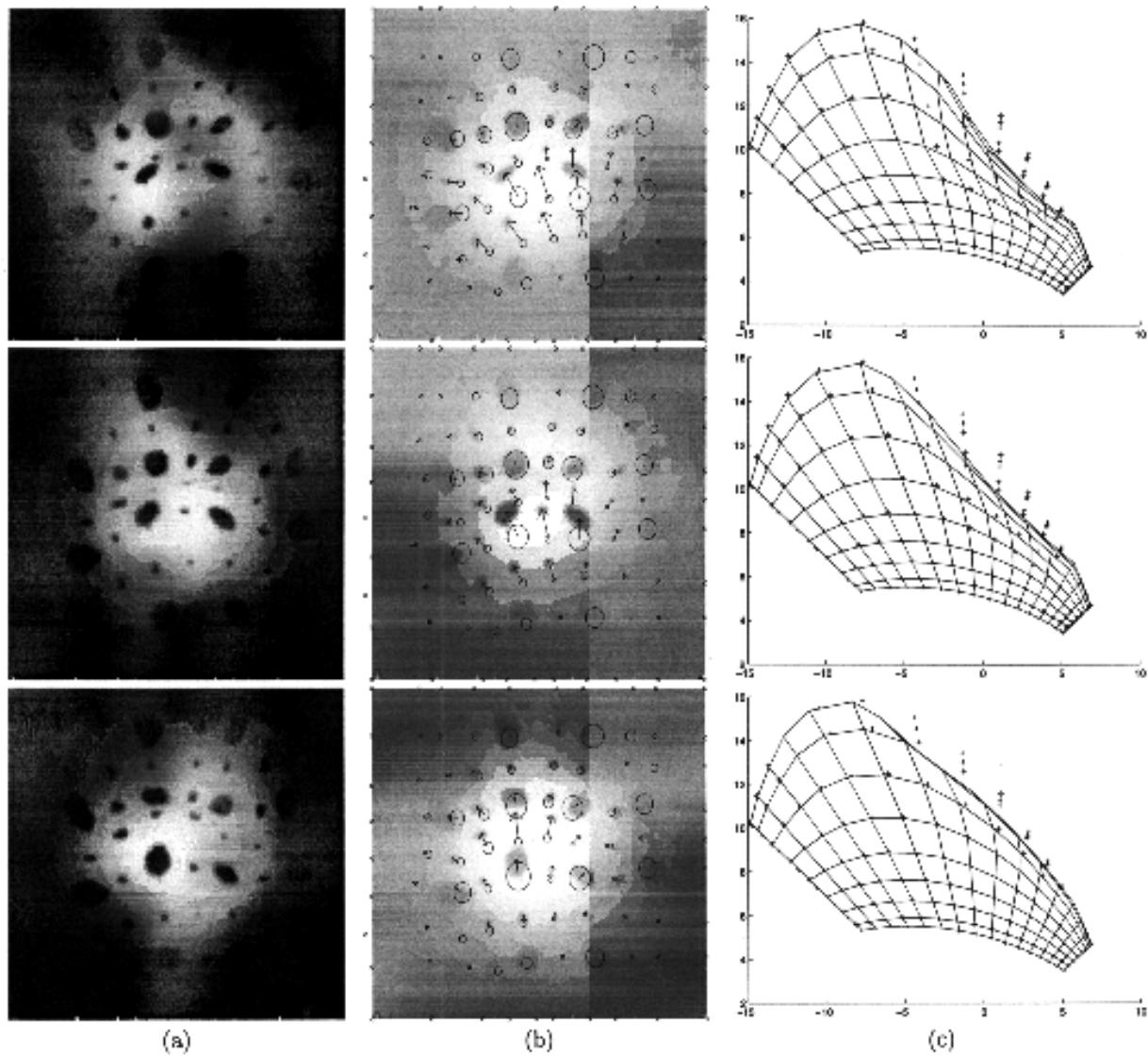
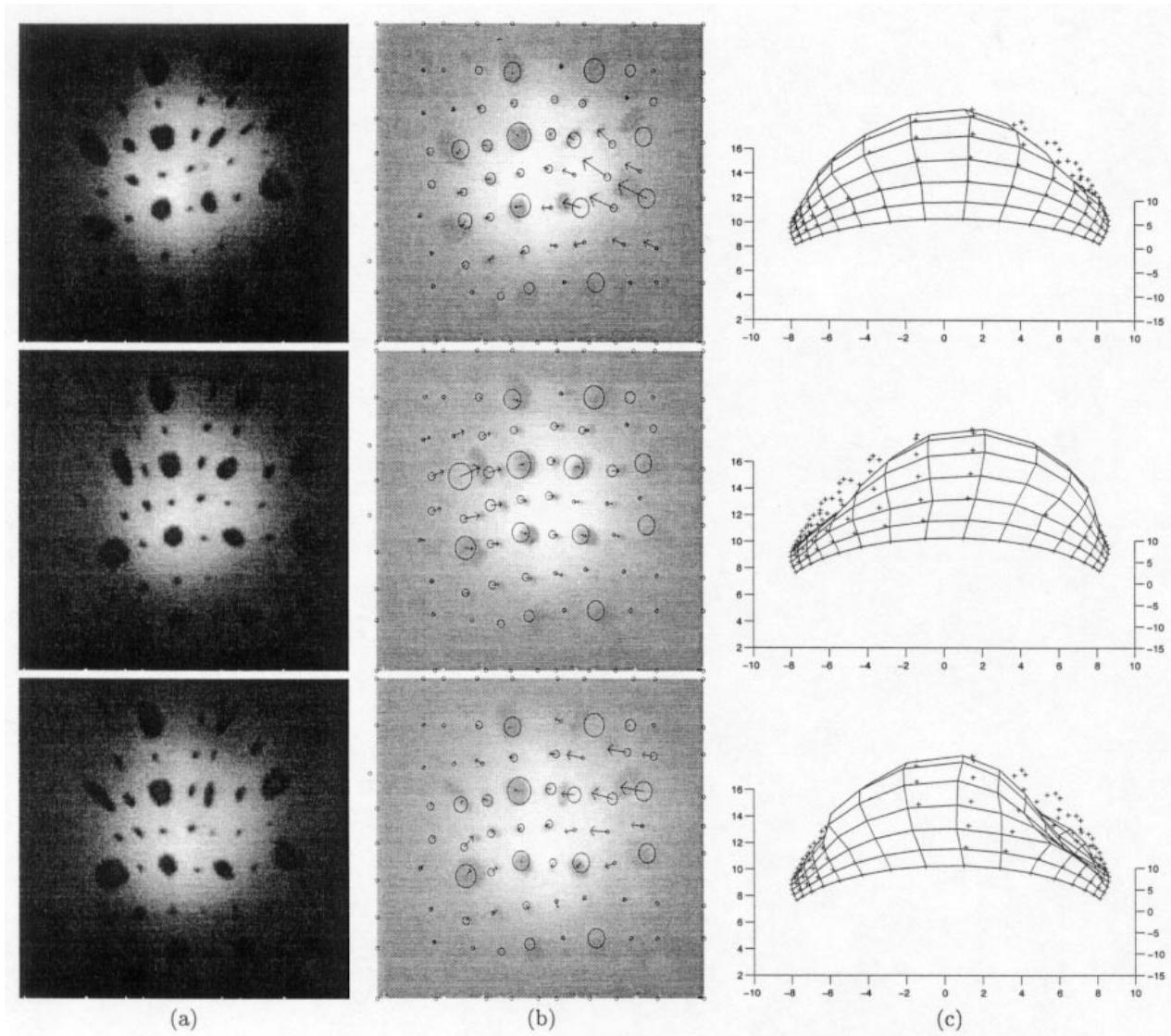Fig. 12. (a) deformed images (b) blob matches (c) reconstruction

Fig. 13. (a) deformed image (b) all blob matches (c) reconstructed finger shape
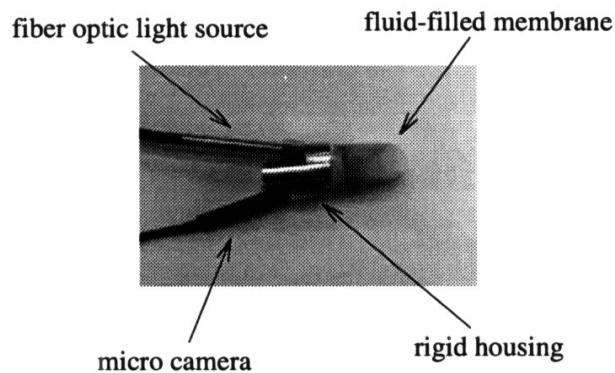

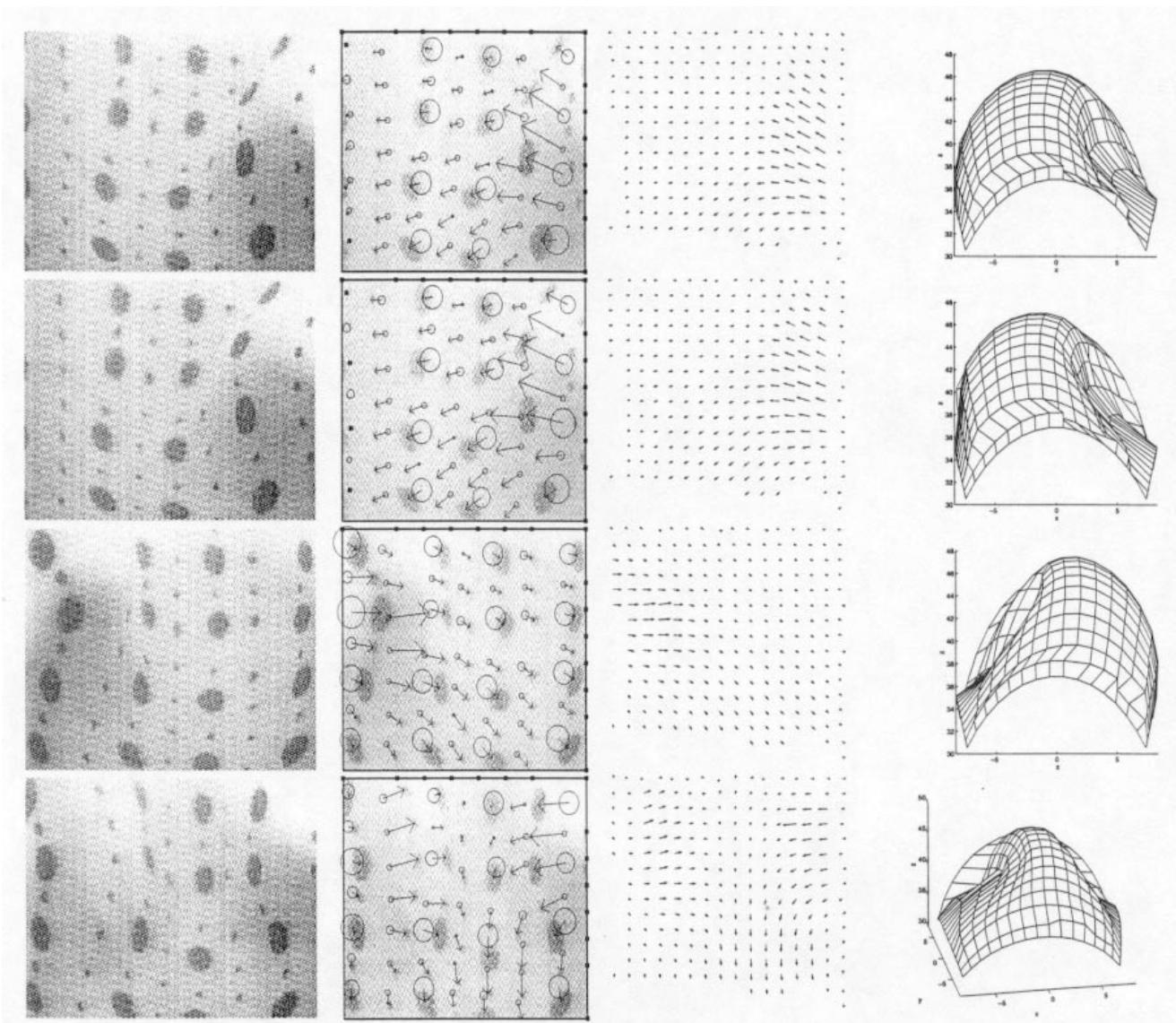Fig. 14. A second-generation finger sensor using membrane shape reconstruction.

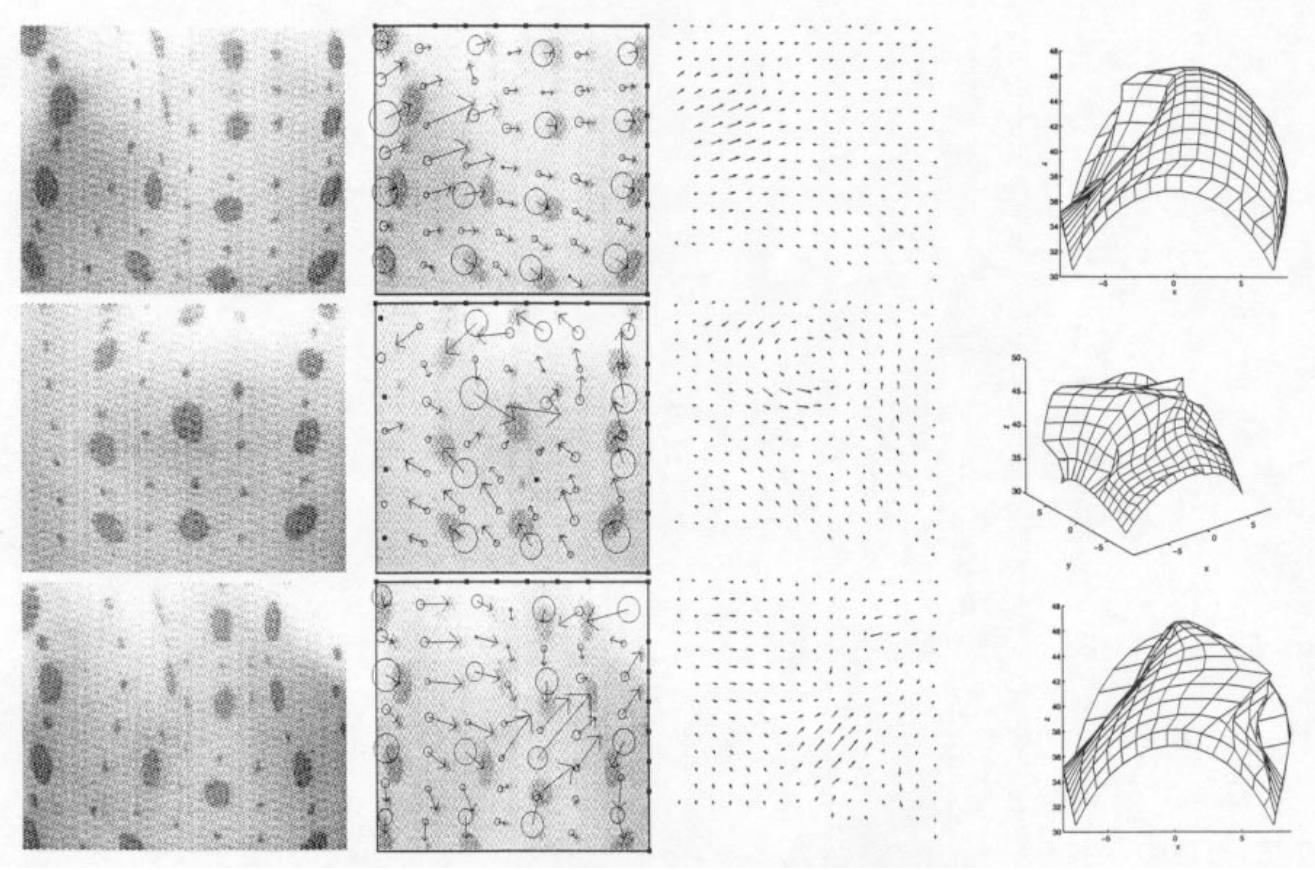Fig. 15. Reconstruction using second-generation finger.

Fig. 16. Problem reconstructions—if the image matching is not correct, the reconstruction produces unreliable results.

6. Summary

In this paper, we have described a physical situation in which the shape of a membrane is to be inferred from an image of it. Based on the principal that under distortion the true membrane shape will minimize the energy stored in the membrane, we presented an algorithm to reconstruct the shape of a membrane. Physical principles lead to a set of nonlinear partial differential equations, and an approximate solution is found using linearization.

We measured the projections on the image plane of markings on the surface of the membrane. A good approximation to the shape of the nominal membrane is required, and we presented a method to achieve this. Experimental results showed that membrane shape and contact location can be successfully determined. It is the subject of ongoing work to use this shape information for grasping applications.

Appendix A: One-Dimensional Membrane Mechanics

This section presents the membrane reconstruction problem in one dimension to prepare the reader and motivate the concepts and ideas used in the 2d case.

Object Contact with Flat 1d Membrane

Consider a horizontal line with end-point 0 and a. Consider a one-dimensional membrane (e.g., a rubber band) fixed at 0 and a. Let the height of the membrane be $u(x)$ for $0 \leq x \leq a$. Of course, u is continuous. If there is contact with an object having a smooth boundary, the minimum energy solution will yield a differentiable u. Figure 8 depicts a situation in which the shape of the contact boundary of the object is given by $y = \psi(x)$ $c_1 \leq x \leq c_2$, where $\psi(x) = 0$ for some $x \in [c_1, c_2]$. We need to include a constraint on the volume of the membrane cavity. Hence, with a maximum depression of α, the contact boundary of the object and membrane is described by $y = \psi(x) - \alpha$ for $c_1 \leq x \leq c_2$ (see Fig. 17). The membrane position $y = u(x)$ obeys the minimum energy solution on the noncontact domains $0 \leq x \leq c_1$ $c_2 \leq x \leq a$. Conditions of transversality from the calculus of variations imply that the tangent of the membrane matches the tangent of the object at points of control. To determine the shape of the membrane $u(x)$, we solve

$$\inf_u \tau/2 \int_0^a \left(\frac{du}{dx} \right)^2 dx \quad \text{such that} \qquad (30)$$
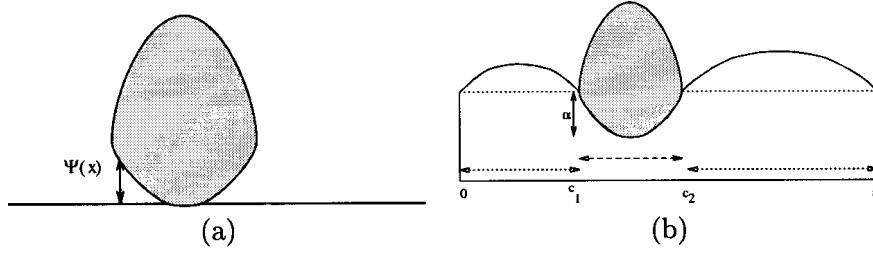
Fig. 17. (a) A convex object defined by function $\psi(x)$ where $\psi(x) = 0$ for some x in contact with the membrane(b) with a maximum displacement of α, then the portion of the membrane in contact with the object is defined by $u(x) = \psi(x) - \alpha$.

$$u(0)=u(a)=0, \quad u(x)=\psi(x)-\alpha, \ c_1 \leq x \leq c_2,$$
$$\text{(boundary)} \qquad\qquad \text{(object shape)}$$

$$u_x(c_i)=\psi_x(c_i), \text{ for } i=1,2, \qquad 0=\int_0^a u\,dx$$
$$\text{(transversality)} \qquad \& \qquad \text{(volume)} \ . \tag{31}$$

Because we do not have an a priori description of the object ψ, we must simultaneously determine the points of contact and the shape. The membrane minimizes the elastic energy in the portions of the membrane that are *not* in contact with the object: we assume that the segments of the membrane in contact with the object conform to the shape of the object.

Reconstruction with Nonflat 1d Membrane

Consider a semicircular 1d membrane that is deformed by contact with an object of zero width, the location and depth of which is unknown. We *observe* the projection of points drawn on the membrane. Model the deformation by

$$\phi : r(\theta) \rightarrow u(\psi). \tag{32}$$

The difference $\theta - \psi$ is determined from the image, see Figure 18.

Given the related pairs ψ_i and θ_i, we interpolate to obtain the intermediate points and represent this relationship at $g(\theta) = \psi$.

The metric of the deformed membrane manifold is

$$H = u^2 + (\frac{du}{d\psi})^2, \tag{33}$$

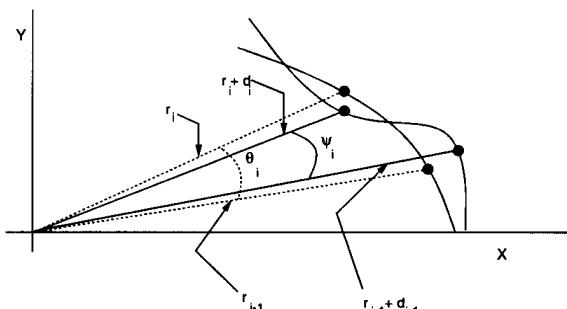Fig. 18. Imaging in 1D.

where $u(\psi) = r(g^{-1}(\psi)) + \phi(g^{-1}(\psi))$. Because we observe only the projection of the membrane points, $\phi(g^{-1}(\psi))$ is unknown. The deformation $\phi = u - r$ (i.e., the radial displacement) is to be recovered. For the given geometry of the undeformed membrane, we will assume a semicircular shape. Get the radius of the semicircle to tear. In this case, the metric on N is

$$H = u^2 + (\frac{du}{d\psi})^2 = (r + \phi)^2 + (\frac{dr}{d\psi} + \frac{d\phi}{d\psi})^2$$
$$= (r + \phi)^2 + (\frac{d\phi}{d\theta})^2(\frac{d\theta}{d\psi})^2 \tag{34}$$

and the Jacobian is $J = (\frac{d\phi}{d\theta})$. The harmonic map functional is

$$J^2 H G^{-1} = \frac{1}{r}(\frac{d\phi}{d\theta})^2[(r + \phi)^2 + (\frac{d\phi}{d\theta})^2(\frac{d\theta}{d\psi})^2], \tag{35}$$

so the equilibrium configuration will be described by the ϕ that minimizes

$$\eta = \int \frac{1}{r}(\frac{d\phi}{d\theta})^2[(r + \phi)^2 + (\frac{d\phi}{d\theta})^2(\frac{d\theta}{d\psi})^2]\frac{1}{\sqrt{r}}d\theta. \tag{36}$$

Of course, the integration is over the regions of the membrane not in contact with the object and the minimization is subject to the constraints on the volume,

$$\int r^2 d\theta = \int u(\psi)^2 d\psi \ \text{ and } \ u(0) = 0, \quad u(\pi) = 0. \tag{37}$$

1D Reconstruction Using Grid Approximation

To obtain data to test the 1D reconstruction, we built a fluid-filled half-cylinder device covered (on the curved portion of the half-cylinder) with a rubber membrane. A one-dimensional cross section provides data for a 1d membrane. The area under a cross section in the center of the device is approximately constant (the length of the cylinder was made much larger than the diameter to justify this assumption). The original membrane shape was a semicircle. The image displacement of a pattern drawn on the membrane was measured. Figures 19 and 20 show reconstruction results.
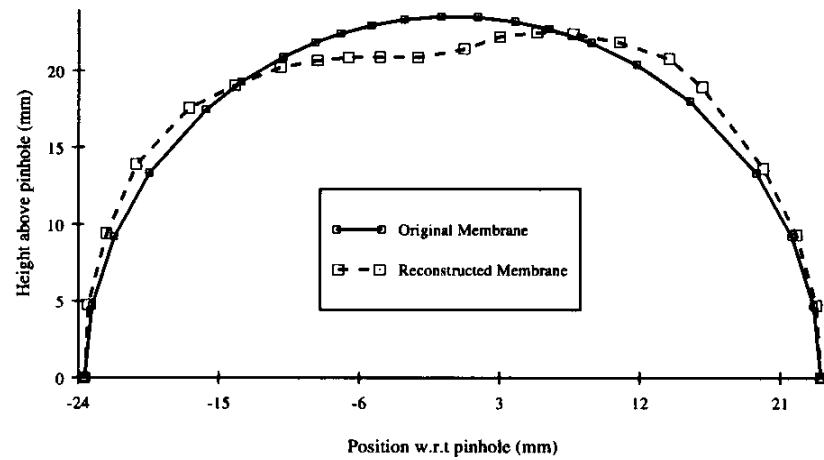
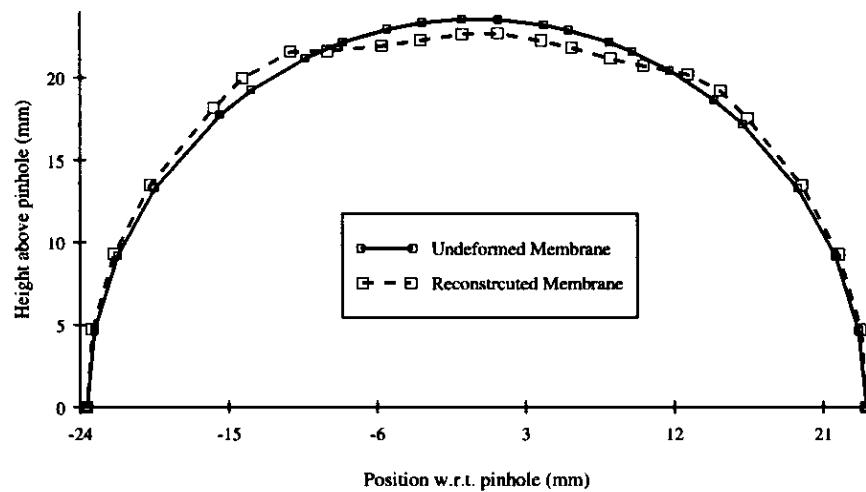Fig. 19. 1D reconstruction: contact with membrane with cylindrical object—actual depression was ≈ 4 mm.

Fig. 20. 1D reconstruction: contact with membrane at two separate points—actual depression was 2 mm.

Appendix B: Two-Dimensional Membrane Mechanics

The elementary treatment of flat membranes with small displacements as carried out in, e.g., Courant and Hilbert (1953) leads to the conclusion that the normal displacement satisfies Laplace's equation subject to boundary conditions. Here we have a more complicated situation and must use an expression for the energy associated with stretching, which takes into consideration the underlying geometry of the undeformed membrane. An analysis of an object in contact with a flat membrane can be found in Elliott and Friedman (1986).

In studying membrane mechanics, one can take either an extrinsic or an intrinsic point of view. In the former, the membrane is described as a surface in three-dimensional space and deformations are specified in terms of a fixed three-dimensional coordinate system. The second point of view treats each state of deformation as a two-dimensional manifold, and the energy is expressed in terms of the mapping ϕ, which takes one deformed state into another. This second point of view can be called intrinsic. If one is interested in small deformations from a simple geometry (e.g., an initially flat membrane), the first point of view is most transparent. However, the second is a simpler statement of the intrinsic principle. Our analysis uses both. Let the surface of the undeformed membrane be identified with a manifold M. We regard M as a Riemannian manifold with metric, G, inherited from the ordinary three-dimensional space. Likewise, the surface of the deformed membrane is identified with a manifold N. The deformation is described by the mapping

$$\phi : M \to N. \tag{38}$$

The boundary of M remains fixed; thus, M and N share a common boundary (i.e., $\phi(p) = p$ for $p \in \partial M$). The differential, $d\phi$, is a mapping of the tangent space of M at p to the tangent space of N at $\phi(p)$ denoted:

$$d\phi : T_p M \to T_{\phi(p)} N. \tag{39}$$

Choosing local coordinates[1] $\{x^1, \ldots, x^m\}$ for $p \in M$ and $\{y^1, \ldots, y^n\}$ for $\phi(p) \in N$, the tangent spaces will have coordinate bases $\{\frac{\partial}{\partial x^i}\}$ at p and $\{\frac{\partial}{\partial y^a}\}$ at $\phi(p)$, and we denote the matrix of $d\phi()$ with respect to these bases by $J = [J_{ai}]$:

$$J = \left[\frac{\partial \phi^a}{\partial x^i}\right]. \tag{40}$$

For a vector $X \in T_p(M)$, the energy density is defined by Eells and Sampson (1964)

$$e(\phi) = \frac{1}{2}\|d\phi(X)\|^2 = \frac{1}{2}\text{tr}(\phi^* H)(p) \tag{41}$$

where $\| \cdot \|$ denotes the induced tensor norm on $T_p^*(M) \times T_{\phi(p)}N$, sometimes called the pullback metric. The metric is one half of the sum of the eigenvalues of the first fundamental form on $T_p(M)$ with respect to G. In coordinates, the energy density is expressed using summation notation as

$$e(\phi) = \frac{1}{2}G^{ij} H_{ab}(\phi(p))\frac{\partial \phi^a}{\partial x^i}\frac{\partial \phi^b}{\partial x_j} = \frac{1}{2}\text{tr}[J^T H J G^{-1}], \tag{42}$$

where the latter equality is an equivalent energy density expression[2] called the harmonic map functional (Park and Brockett 1994).

To get a physical interpretation of the energy density, we consider the polar decomposition of J: $J = RU = VR$, where $R : TM \to TN$ is an orthogonal transformation (i.e., $R^T R = I$) and U and V are symmetric positive definite matrices (called the stretch tensors). The eigenvalues of U are called the right *principal stretches* (and the eigenvalues of V are called the left principal stretches). Geometrically, the stretch tensors measure changes in lengths (and angles) due to the deformation ϕ. The deformation tensor is defined by (see Marsden and Hughes 1983):

$$C(p, W) = (p, d\phi(X)^T d\phi(X)W) \tag{43}$$

where $W \in T_p(M)$. In coordinates $\{x^i\}$ and $\{y^a\}$ on M and N, respectively,

$$C_{AC} = H_{ab}\frac{\partial \phi^b}{\partial x^A}\frac{\partial \phi^a}{\partial x^C}, \tag{44}$$

which when expressed with respect to G are the components of the first fundamental form $(\phi^* H)(x)$. Hence, the energy density (eq. (41)) is the trace of the deformation tensor. The polar decomposition of C is $C = J^T J = U^T R^T RU = U^T U$. The deformation tensor, C, has eigenvalues that are squares of the principal stretches. At each point on M, the stretch tensor measures the squares of the changes in length in the principal directions at that point. The material (Lagrangian) strain tensor is defined by $2E = C - I$. If $C = I$ (an isometry), then $E = 0$ and points on M experience no relative motion (deformation or stretching) under ϕ. We can interpret the energy density as measuring the strain at a point on M. The total energy associated with the mapping ϕ is

$$E(\phi) = \int_M e(\phi)dV_M, \tag{45}$$

where dV_M is the volume element of M. Thus, the total energy, $E(\phi)$, can be interpreted as the sum of the strains over the manifold or as the "average" strain. A spring stores energy under deformation from its nominal length, and the stored

---

1. Here we are using manifolds of dimension m and n. In practice, we have a two-dimensional membrane, hence $\dim M = \dim N = 2$.

2. This follows easily: $2e(\phi) = \text{tr}[G^{-1}J^T H J] = [G^{-1}J^T H J]_{ii} = G^{ij}J_{bj}H_{ba}J_{ai} = G^{ij}H_{ab}J_{ai}J_{bj}$.
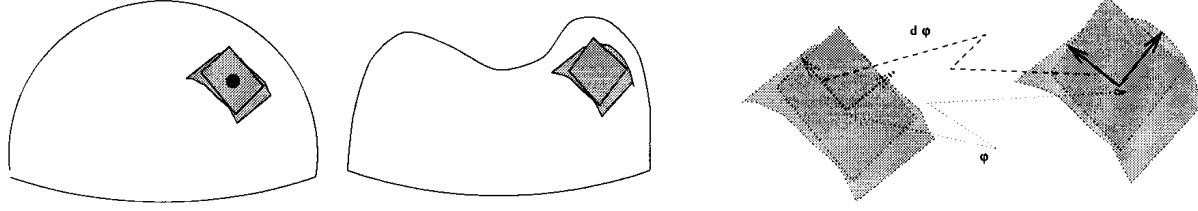
Fig. 21. Manifold mapping of one membrane deformation state into another.

energy is proportional to the square of the change in length of the spring. The membrane energy stored expressed as (45) agrees with this intuitive notion that the energy of a membrane is "spring-like" and energy is proportional to the squares of the changes in length of the "springs" in the principal directions. It should be noted that this elastic model also "stores" energy under compression. A membrane does not store energy when compressed; in fact, in our laboratory measurements, it was difficult to compress the membrane (it bends and/or buckles). However, for the tactile sensor application we are considering, the membrane will be subjected *only* to stretching and not to compression. We can apply this model because it is accurate for the motions we anticipate.

There is much literature on the numerical solution of partial differential equations with boundary values, or the equivalent minimization problems, using grid approximations (e.g., Vemuri and Karplus 1981). The methods reduce the solution of the partial differential equations to a set of algebraic equations. Our equations are nonlinear; we work with linear approximations.

Boundary Conditions

The external membrane boundary is fixed, hence boundary points do not move, $\phi(p) = p$ for $p \in \partial M$. Let $M_C \subset M$ be the portion of M in contact with the object and denote the portion of M not in contact with the object by $M \setminus M_C$. We call the boundary of M_C and $M \setminus M_C$ the *interior* boundary or the contact boundary. If M_C is a nondegenerate subset of M (i.e., not a point contact), then the membrane is C^1 continuous at the contact boundary (Elliott and Friedman 1986). However, the interior boundary (of $M \setminus M_C$) is not known precisely. It is expected that M_C take a shape that is related to the shape of the object in contact with the membrane. We do not know anything about that shape. We do, however, have interior point constraints from the imaging, as described earlier.

Appendix C: Details of the Affine Matching Computation

In this appendix, we derive the expression for the best fit affine transformation between two point sets in R^3 (although extensions to other dimensions are clear). We define a least squares

matching criteria that minimizes the Euclidean distance between two point sets as

$$||Ax_i - b - y_i||^2 = \sum_i [Ax_i - b - y_i]^T \mathbf{Q} [Ax_i - b - y_i],$$
(46)

where $A \in R^{3 \times 3}$, $b \in R^3$, and $\mathbf{Q} \in R^{3 \times 3}$ is a positive definite symmetric matrix (it could represent the uncertainty in the points and/or the point correspondences). Here, we take $\mathbf{Q} = I$.

Brockett (1989) described general least square matching for the pair (A, b) in one of the matrix subgroups of the general linear group. We follow this approach investigating the simple case for affine matching between point sets in R^3.

Given n point matches, we rewrite the matching criteria as

$$\eta(A, b) = \sum_{i=1}^n [Ax_i - b - y_i]^T [Ax_i - b - y_i]$$

$$= \sum_{i=1}^n \left[x_i^T A^T A x_i - 2x_i^T A^T b - 2x_i^T A^T y_i \right.$$

$$\left. + 2y_i^T b + b^T b + y_i^T y_i \right].$$

Since the last term is fixed and will not affect the minimization, we will neglect it in further calculations. The minimum value of η with respect to b will occur for $\frac{\partial \eta}{\partial b} = 0$. Performing this computation leads to

$$b_o = A\bar{x} - \bar{y},$$
(47)

where

$$\bar{x} = \frac{1}{n} \sum_{i=1}^n x_i \quad \text{and} \quad \bar{y} = \frac{1}{n} \sum_{i=1}^n y_i.$$
(48)

Let

$$F = (\sum_i x_i \cdot y_i^T) - n\bar{x}\bar{y}^T \quad \text{and}$$

$$G = (\sum_i x_i \cdot x_i^T) - n\bar{x}\bar{x}^T,$$
(49)

and use the fact that for square matrices AB and A, $\text{tr}[AB] = \text{tr}[BA]$ and $\text{tr}[A^T] = \text{tr}[A]$ to determine the following modified matching criteria (neglecting terms not dependent on A):

$$\tilde{\eta}(A) = \text{tr}[AGA^T - 2AF] \tag{50}$$

which we seek to minimize (over A). Perturbing A to $A(I + \epsilon L)$ and expanding yields

$$
\begin{aligned}
\tilde{\eta}(A(I + \epsilon L)) &= \text{tr}[GA^T A - 2FA + \epsilon(GA^T AL \\
&\quad + GL^T A^T A - 2FAL) \\
&\quad + \epsilon^2 GL^T A^T AL] \\
&= \tilde{\eta}(A) + \epsilon\,\text{tr}[GA^T AL \\
&\quad + GL^T A^T A - 2FAL] + h.o.t. \\
&\approx \tilde{\eta}(A) + 2\epsilon\,\text{tr}[GA^T AL - FAL].
\end{aligned}
$$

Then, to *first order* in ϵ, A_o is a critical point of $\tilde{\eta}(A)$ if

$$\text{tr}[(GA_o^T A_o - FA_o)L] = 0. \tag{51}$$

For arbitrary L, eq. (51) has many possible choices for A. In the general case, setting $(GA^T A - FA) = 0$ does not ensure that A will be a transformation of the required form (for example, if one required A to be orthogonal). However, the pair (A_o, b_o) will define an affine transformation as long as A is nonsingular. In this case, setting $GA_o^T A_o - FA_o = 0$ and taking the solution

$$GA^T A = FA \quad \rightarrow \quad A = F^T G^{-1} \tag{52}$$

yields a nonsingular matrix A for nonsingular F and G.

For our purposes, A is nonsingular as long as the four points defining a quadrilateral on the membrane are not collinear. The components of A are

$$A_{ij} = \frac{1}{\det G} \sum_{k=1}^{3} F_{ki}\,\text{adj}\,G_{kj}. \tag{53}$$

In the context of matching the points on the grid of the elastic membrane, g_{ij} are *known* values and f_{ij} are the *unknowns*, hence A_{ij} are linear expressions in the unknown parameters.

Appendix D: Expressing the Approximation to the Harmonic Map Functional as a Quadratic Form

In Section 3.1, we derived the discrete approximation to the harmonic map functional (eq. (12), repeated here)

$$E(\phi, \psi) \approx \sum_{ij} \left[\text{tr} A_{ij}^T H A_{ij} G^{-1}\, area_{ij} \right] + \xi. \tag{54}$$

For $A_{ij} = [a_{kl}]$, the expression $\text{tr}\,A_{ij}^T H A_{ij} G^{-1}$ at for the ijth quadrilateral is (dropping the subscript ij for readability)

$$
\begin{aligned}
\text{tr}[A^T & HAG^{-1}]_{ij} = \\
& \left(a_{12}^2(1 + s_x^2) + a_{11}^2(1 + s_y^2) - 2a_{11}a_{12}s_x s_y \right) \\
& \left(1 + s_x^2 + 2s_x\psi_x + \psi_x^2 \right) \\
& + \left(a_{22}^2(1 + s_x^2) + a_{21}^2(1 + s_y^2) - 2a_{21}a_{22}s_x s_y \right) \\
& \left(1 + s_y^2 + 2s_y\psi_y + \psi_y^2 \right) \\
& + 2 \left(a_{12}(a_{22} + a_{22}s_x^2 - a_{21}s_x s_y) \right. \\
& \left. + a_{11}(a_{21} - a_{22}s_x s_y + a_{21}s_y^2) \right) \\
& \left((s_x + \psi_x)(s_y + \psi_y) \right),
\end{aligned}
\tag{55}
$$

which we can write as

$$
\begin{bmatrix} \psi_x, & \psi_y, & 1 \end{bmatrix}
\begin{bmatrix} m_{xx} & \frac{1}{2}m_{xy} & m_x \\ \frac{1}{2}m_{xy} & m_{yy} & m_y \\ 0 & 0 & m_0 \end{bmatrix}
\begin{bmatrix} \psi_x \\ \psi_y \\ 1 \end{bmatrix}, \tag{56}
$$

where

$$m_{xx} = a_{12}^2(1 + s_x^2) - 2a_{11}a_{12}s_x s_y + a_{11}^2(1 + s_y^2) \tag{57}$$

$$m_{yy} = a_{22}^2(1 + s_x^2) - 2a_{21}a_{22}s_x s_y + a_{21}^2(1 + s_y^2) \tag{58}$$

$$
\begin{aligned}
m_{xy} = 2(&a_{12}(a_{22} + a_{22}s_x^2 - a_{21}s_x s_y) \\
&+ a_{11}(a_{21} - a_{22}s_x s_y + a_{21}s_y^2))
\end{aligned}
\tag{59}
$$

$$
\begin{aligned}
m_x = 2(&a_{11}^2 s_x(1 + s_y^2) + a_{12}(a_{12}(s_x + s_x^3) \\
&+ s_y(a_{22} + a_{22}s_x^2 - a_{21}s_x s_y)) \\
&+ a_{11}s_y(-(s_x(2a_{12}s_x + a_{22}s_y)) + a_{21}(1 + s_y^2)))
\end{aligned}
\tag{60}
$$

$$
\begin{aligned}
m_y = 2(&a_{12}s_x(a_{22} + a_{22}s_x^2 - a_{21}s_x s_y) \\
&+ a_{11}s_x(a_{21} - a_{22}s_x s_y + a_{21}s_y^2) \\
&+ s_y(a_{21}^2 + a_{22}^2 + a_{22}^2 s_x^2 - 2a_{21}a_{22}s_x s_y + a_{21}^2 s_y^2))
\end{aligned}
\tag{61}
$$

$$
\begin{aligned}
m_0 = &a_{12}^2(1 + s_x^2)^2 + 2a_{12}s_x s_y(a_{22} + a_{22}s_x^2 - a_{21}s_x s_y) \\
&+ a_{11}^2(1 + s_x^2)(1 + s_y^2) - 2a_{11}s_x s_y(a_{12} - a_{21} \\
&+ a_{12}s_x^2 + a_{22}s_x s_y - a_{21}s_y^2) + (1 + s_y^2) \\
&(a_{21}^2 + a_{22}^2 + a_{22}^2 s_x^2 - 2a_{21}a_{22}s_x s_y + a_{21}^2 s_y^2).
\end{aligned}
\tag{62}
$$

When we use discrete approximations to the partial derivatives in eq. (10), $[\psi_x, \psi_y]$ at vertex ij can be expressed in terms of ψ_{ij}, $\psi_{i+1,j}$, and $\psi_{i+1,j+1}$. Recall we defined the vector $\hat{\psi} = [\psi_{11}, \ldots, \psi_{1n}, \ldots, \ldots, \psi_{mn}]$ whose components are discrete values of the incremental shape map, indexed by their grid position. The matrix in (56) expands to $\tilde{\psi}^T M \tilde{\psi}$, where

$\tilde{\psi}^T = (\ldots, \psi_{ij}, \psi_{i\ j+1}, \ldots, \psi_{i+1\ j}, \ldots, 1)^T$ and M is

$$
\begin{bmatrix}
\ddots & \vdots & & \vdots & \\
& m_{xx}+m_{yy}+m_{xy} & m_{yy}+\frac{1}{2}m_{xy} & \cdots \\
& m_{yy}+\frac{1}{2}m_{xy} & m_{yy} & \cdots \\
& \vdots & \vdots & \ddots \\
& m_{xx}+\frac{1}{2}m_{xy} & \frac{1}{2}m_{xy} & \cdots \\
& \vdots & \vdots & \ddots \\
& 0 & 0 &
\end{bmatrix}
\tag{63}
$$

$$
\begin{bmatrix}
\vdots & & \vdots \\
m_{xx}+\frac{1}{2}m_{xy} & \cdots & 0 \\
\frac{1}{2}m_{xy} & \cdots & m_y \\
\vdots & \ddots & \vdots \\
m_{xx} & \cdots & m_x \\
\vdots & \ddots & \vdots \\
0 & & m_0.
\end{bmatrix}
$$

From expressions (12) and (63), we see that the approximate formula for E can be organized in terms of the sum of quadratic terms in ψ_{ij} and quadratic terms in A_{ij} (the projection of ϕ), plus higher order terms, which we will ignore. By incorporating the contributions from each quadrilateral (multiplied by the area term) and after some rearranging and grouping of terms, we can rewrite the energy as a quadratic form

$$
E(\hat{\psi}) = \| Q\hat{\psi} - \boldsymbol{\gamma} \|^2. \tag{64}
$$

Acknowledgments

References

Akella, P., and Cutkosky, M. 1989. Manipulation with soft fingers: Modeling contacts and dynamics. *Proceedings of the IEEE Int. Conference on Robotics and Automation*, Scottsdale, AZ, pp. 764–769.

Beardsley, P., and Zisserman, A. 1995. Affine structure from motion. *Proc. 4th Int. Conf. on Computer Vision*, Boston, MA, pp. 58–64.

Belhumeur, P. 1993. A binocular stereo algorithm for reconstructing sloping, creased, and broken surfaces in the presence of half-occlusion. *Proc. 3th Int. Conf. on Computer Vision*, Berlin, Germany, pp. 431–438.

Bennett, B., Hoffman, D., Nicola, J., and Prakash, C. 1989. Structure from two orthographic views of rigid motions. *Journal of the Optical Society of America* 6:1052–1069.

Brockett, R. W. 1985. Robotic hand with rheological surfaces. *Proceedings of the 1985 IEEE Conference on Robotics and Automaton*, Philadelphia, PA, pp. 942–946.

Brockett, R. W. 1989. Least squares matching problems. *Linear Algebra and Its Applications* 124:761–777.

Chang, D., and Cutkosky, M. 1995. Rolling with deformable fingertips. *Proceedings of the IEEE Int. Conference on Intelligent Robots and Systems*, Pittsburgh, PA, pp. 194–199.

Courant, R., and Hilbert, D. 1953. *Methods of Mathematical Physics*, vol. 1. New York: John Wiley.

Eells, J., and Lemaire, L. 1978. A report on harmonic maps. *Bulletin of the London Mathematical Society* 10:1–68.

Eells, J., and Sampson, J. H. 1964. Harmonic mappings of Riemannian manifolds. *Journal of the American Mathematical Society* 86:109–160.

Elliott, C. M., and Friedman, A. 1986. The contact set of a rigid body partially supported by a membrane. *Nonlinear Analysis, Theory, Methods & Applications* 10(3):251–276.

Harris, C. 1992. Geometry from visual motion. In *Active Vision*, ed. A. Blake and A. Yuille, 263–284. Cambridge, MA: MIT Press.

Horn, B. 1986. *Robot Vision*. New York: McGraw-Hill.

Hristu, D. 1999. Optimal Control with Limited Communication. Ph.D. thesis, Harvard University, Cambridge, MA.

Kao, I., and Cutkosky, M. 1993. Comparison of theoretical and experimental force/motion trajectories for dexterous manipulation with sliding. *The International Journal of Robotics Research* 12(6):529–534.

Koenderink, J., and Van Doorn, A. 1991. Affine structure from motion. *Journal of the Optical Society of America* 8(2):377–385.

Lipson, P., Yuille, A., Keeffe, D., Cavanaugh, J., Taaffe, J., and Rosenthal, D. 1990. Deformable templates for feature extraction from medical images. In *Proc. 1st European Conference on Computer Vision*, ed. O. Faugeras, 413–417. New York: Springer-Verlag.

Lowe, D. 1992. Robust model-based motion tracking through the integration of search and estimation. *Int. Journal of Computer Vision* 8(2):113–122.

Maekawa, H., Komoriya, K., and Tanie, K. 1992. Manipulation of an unknown object by multifingered hands with rolling contact using tactile feedback. *Proceedings of the IEEE Int. Conference on Intelligent Robots and Systems*, Raleigh, NC, pp. 1877–1882.

Marsden, J. E., and Hughes, T. J. 1983. *Mathematical Foundations of Elasticity*. Englewood Cliffs, NJ: Prentice Hall.

Montana, D. 1988. The kinematics of contact and grasp. *Int. Journal of Robotics Research* 7(3):17–32.

Montana, D. 1989. The kinematics of contact with compliance. *Proceedings of the IEEE Int. Conference on Robotics and Automation*, Scottsdale, AZ, pp. 770–774.

Nowlin, W. 1991. *Tactile Sensors with Compliant Manipulators*. Ph.D. thesis, Harvard University, Cambridge, MA.

Park, F., and Brockett, R. W. 1994. Kinematic dexterity of robotic mechanisms. *Int. Journal of Robotics Research* 13(1):1–15.

Perkins, W. 1978. A model-based system for industrial parts. *IEEE Trans. Comp.* 27(2):126–143.

Son, J., Monteverde, E., and Howe, R. 1994. A tactile sensor for localizing transient events in manipulation. *Proceedings of the IEEE Int. Conference on Robotics and Automation*, San Diego, CA, pp. 471–476.

Terzopoulos, D., Witkin, A., and Kass, M. 1987. Symmetry-seeking models and 3d object reconstruction. *International Journal of Computer Vision* 1:211–221.

Terzopoulos, D., Witkin, A., and Kass, M. 1988. Constraints on deformable models: Recovering 3d shape and nonrigid motion. *Artificial Intelligence* 36:91–123.

Tomasi, C., and Kanade, T. 1992. Shape and motion from image streams under orthography: A factorization approach. *Int. Journal of Computer Vision* 9(2):137–154.

Ullman, S., and Basri, R. 1991. Recognition by linear combinations of models. *IEEE Trans. Pattern Analysis and Machine Intelligence* 13(10):992–1006.

Vemuri, V., and Karplus, W. J. 1981. *Digital Computer Treatment of Partial Differential Equations*. Englewood Cliffs, NJ: Prentice Hall.

Verri, A., and Torre, V. 1986. Absolute depth estimate in stereopsis. *Journal of the Optical Society of America* 3(3):297–299.

Yuille, A. 1990. Generalized deformable models, statistical physics, and matching problems. *Neural Computation* 2:1–24.